

Adaptive Motor Control for Human-like Spatial-temporal Adaptation

Xiaofeng Xiong^{1,4} and Poramate Manoonpong^{1,2,3}

Abstract—Human arms can produce stable and variable compliant joint motions to achieve tasks in various spatial tasks and temporal scales. To emulate such motions we propose an adaptive motor controller (AMC) allowing for spatial-temporal adaptation of human-like motor control. The AMC is a biomimetic controller consisting of online force and impedance (i.e., stiffness and damping) adaptation to different tasks and unknown arm dynamics. As a result, the AMC can produce more accurate and stable human-like reaching and tracking behaviors, compared to conventional controllers. Moreover, the reproduced spatial-temporal adaptation is comparable to that found in the experiments of human motor control. The proposed AMC may pave a novel and simple way forward to understanding and solving inverse dynamics and variable impedance control in robotics and biomechanics.

I. INTRODUCTION

Human sensorimotor systems excel in stable variable compliant behaviors in dynamic and unpredictable environments [1], [2], [3], [4]. Whereas most robots are still controlled by high gain negative error feedback control (e.g., PD control) [5], [6]. Humans are capable of utilizing previously learned motor skills in various (e.g., spatial or temporal) contexts than in that of initial acquisition [7]. This character refers to the spatial-temporal adaptation from one motor task or context to another, i.e., knowledge shared between spatially-temporally different tasks or contexts. For example, humans performed directional reaching and circular tracking in different time scales, leading to adaptive motor behaviors in different spatial-temporal contexts [8]. It has been shown that the human central nervous system (CNS) adapts force and impedance control to various, spatial-temporal tasks [1]. Many researchers have explored the advantages of variable force and impedance control in various tasks. Such control allows not only for different (e.g., temporal) task contexts, but also for flexible applications to different robots.

Variable force and impedance control has been mainly studied through reinforcement learning (RL) [5], [9], operational space control (OSC) [10], [11], [12], optimal control [13], [14], [15], and adaptive control [2], [3], [4]. For

This research is supported by the Human Frontier Science Program (Grant no. RGP0002/2017) and the Thousand Talents Program of China, as well as was funded by the German Research Foundation (DFG) and the National Science Foundation of China (NSFC) under the Crossmodal Learning project, TRR-169.

¹the Embodied AI and Neurorobotics Lab, Centre for Biorobotics, the Mærsk Mc-Kinney Møller Institute, the University of Southern Denmark, 5230 Odense M, Denmark. xizi@mmmi.sdu.dk, poma@mmmi.sdu.dk

²The Institute of Bio-inspired Structure and Surface Engineering, Nanjing University of Aeronautics and Astronautics, Nanjing, China.

³the Bio-inspired Robotics and Neural Engineering Lab, Vidyasirimedhi Institute of Science and Technology (VISTEC), Thailand.

⁴the Department of Informatics, University of Hamburg, Germany.

instance, Rajeswaran et al. (2017) proposed an approach of natural policy gradient based on RL, resulting in a variety of continuous motor control tasks (e.g., hopping) [9]. However, such generalized control can not solve the problem of guaranteeing executional stability of learned tasks with variable impedance [6]. Based on PD control resulting stable motion executions, Mistry and Righetti (2011) developed a new method to derive OSC for constrained under-actuated robots, increasing OSC's computational efficiency in controlling a simulated and three-joint robot [10]. However, the impedance (i.e., stiffness and damping) parameters were not learned in the task, preventing its application to different tasks. To online learn impedance parameters of a two-link robot, Braun et al. (2012) presented an optimal stiffness controller for explosive movement tasks (e.g., throwing balls) [13]. The controller is based on the iterative linear quadratic regulator (iLQR) framework that exploits local state-output approximations and nonlinear robust control, leading to control adaptations to different robot configurations and task contexts [14], [15]. However, the iLQR is prone to be computationally expensive in continuous motor control tasks, as an extension of the linear quadratic regulator (LQR) and differential dynamic programming (DDP). To achieve inexpensive and adaptive impedance control, Smith et al. (2015) presented a hybrid adaptive controller for compliant movements of a simulated Baxter arm [4], [3]. However, such adaptive control relies highly on gains for achieving stable executions in different tasks [6]. For detailed introductions of related works can be seen in [6], [5]. Overall, developing a stable, computationally inexpensive, and simple (e.g., less gain dependence) controller for human-like impedance adaptation is an unsolved problem.

To tackle the problem we propose an adaptive motor controller (AMC) for variable force and impedance control of a simulated human arm (see Fig. 1). The AMC is a biomimetic controller consisting of force and impedance parts that emulate feed-forward and feedback control in human motor control. The learned force and impedance (i.e., stiffness and damping) are online updated by an adaptation law, where the force and impedance adaptation relies mainly on task errors in joint space. The adaptation law is derived from a cost function encoding dynamics adaptation and task parameters, and based on Lyapunov theory.

The main contributions of the proposed AMC include:

- A simple and novel adaptation law allows for stable and variable compliant human-like motor control;
- Such human-like control produce more accurate and stable directional reaching and circular tracking, compared to the implemented OSC and iLQR [11], [14], [15];

- Such human-like control can reproduce spatial-temporal adaptation that is comparable to that found in human motor control and learning [8], [7].

II. HUMAN MOTOR CONTROLLERS

Consider a human arm model with two joints (see Fig. 1), moving it with dynamics [15]:

$$M(q)\ddot{q} + C(q, \dot{q})\dot{q} + G(q) = \tau \quad (1)$$

where $M(q)$ is the positive definite symmetric inertia matrix, q the joint angle vector (i.e., shoulder: q_0 , elbow: q_1), $C(q, \dot{q})\dot{q}$ the torque vector owe to centripetal and Coriolis forces, $G(q)$ the torque vector due to gravity, and τ_u is the joint torques produced by muscles. The matrices and vectors are determined by the kinematics and geometry (see Appendix (IV-A) and Table I [16]) of the human arm. The control laws (i.e., τ in Eq.(1)) of the three human motor controllers are presented and derived for human-like directional reaching and trajectory tracks.

A. Adaptive Motor Controller (AMC)

Inspired by the principles of human motor control [2], [1], the torque $\tau(t) \in \mathbb{R}^{2 \times 1}$ produced by the AMC (see Fig. 1) includes the force and impedance parts:

$$\tau(t) = \underbrace{-F(t)}_{\text{force}} - \underbrace{K(t)e(t)}_{\text{impedance}} - D(t)\dot{e}(t) \quad (2)$$

The position ($e(t) \in \mathbb{R}^{2 \times 1}$), velocity ($\dot{e}(t) \in \mathbb{R}^{2 \times 1}$), and tracking ($\varepsilon(t) \in \mathbb{R}^{2 \times 1}$) errors are given by:

$$e(t) = q(t) - q_d(t), \dot{e}(t) = \dot{q}(t) - \dot{q}_d(t), \varepsilon(t) = e(t) + \beta\dot{e}(t) \quad (3)$$

Suppose that a task is characterized by the trajectory $q_d(t)$ ($t \in [0, T]$), the AMC enables the arm (see Fig. 1) to achieve the task through online adapting the feed-forward force $F \in \mathbb{R}^{2 \times 1}$ and impedance parameters ($K(t) \in \mathbb{R}^{2 \times 2}$ and $D(t) \in \mathbb{R}^{2 \times 2}$). The impedance parameters are the arm stiffness and damping matrices of the human arm (see Fig. 1):

$$K(t) = \begin{bmatrix} k_0(t) & k_1(t) \\ k_2(t) & k_3(t) \end{bmatrix}, D(t) = \begin{bmatrix} d_0(t) & d_1(t) \\ d_2(t) & d_3(t) \end{bmatrix} \quad (4)$$

where $k_{0,1,2,3}(t)$ and $d_{0,1,2,3}(t)$ are dependent on the joint stiffness and damping parameters of the human arm. Their detailed definitions can be seen in [17].

The force (F) and impedance ((K, D)) adaptations are achieved by minimizing task errors and maintaining control stability [18], [2]:

$$J_c(t) = \frac{1}{2} \int_{t-T}^t \|vec(\tilde{K})\|_{Q_k}^2 + \|vec(\tilde{D})\|_{Q_d}^2 + \|\tilde{F}\|_{Q_f}^2 d\sigma \quad (5)$$

utilizing a linear second order impedance model [19] where $\|\cdot\|_{Q_\tau, Q_k, Q_d}$ and $vec(\cdot)$ are the weight norms and column vectorization, while maintaining control stability due to the arm dynamics through:

$$J_p(t) = \int_{t-T}^t \dot{V}(\sigma) d\sigma, V(t) = \frac{1}{2} \varepsilon^T(t) M(q) \varepsilon(t) \quad (6)$$

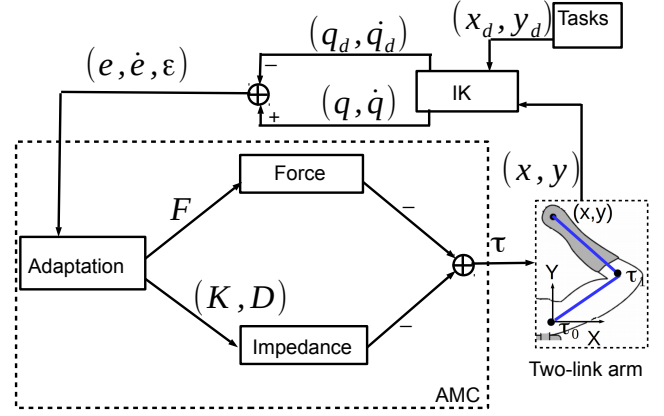


Fig. 1. Adaptive motor controller (AMC). Fed with the errors $(e(t), \dot{e}(t), \varepsilon(t))$ (see Eq.3), the AMC utilizes the adaptation law (see Eq.8) to update its force ($F(t)$) and impedance ($K(t)$ and $D(t)$) parts (see Eq.2), leading to adaptive motions (x, y) to achieve tasks (e.g., tracking desired trajectories) in the Cartesian space. The AMC is a joint space controller that relies on the inverse kinematic (IK) of a two-link human arm [16] (see its geometry parameters in Table I).

The overall minimized cost function is given by:

$$J(t) = J_p(t) + J_c(t) \quad (7)$$

Based on the cost function $J(t)$, the force and impedance adaptation is guided by:

$$F(t) = \frac{\varepsilon(t)}{\gamma(t)}, K(t) = F(t)e^T(t), D(t) = F(t)\dot{e}^T(t) \quad (8)$$

where $\gamma(t)$ is an adaptation scalar with the positive scalars a and b :

$$\gamma(t) = \frac{a}{1 + b\|\varepsilon(t)\|^2} \quad (9)$$

The derivation of the adaptation (i.e., Eq.8) and the scalar values can be seen in Appendix (IV-B).

B. Iterative Linear Quadratic Regulator (iLQR)

The dynamics of the human arm (see Eq.1) can be formulated as:

$$\dot{Z} = AZ + B\tau \quad (10)$$

where

$$Z = \begin{bmatrix} q \\ \dot{q} \end{bmatrix}, A = \begin{bmatrix} 0 & 1 \\ -M^{-1}G & -M^{-1}C \end{bmatrix}, B = \begin{bmatrix} 0 \\ M^{-1} \end{bmatrix} \quad (11)$$

The parameters (e.g., M^{-1}) of the human dynamics are known and took from [15]. Let the deviation from the nominal τ_k and Z_k be $\delta\tau_k$ and δZ_k in terms of the discrete iLQR [15], [14]. The linearization is given by:

$$\delta Z_{k+1} = A_k \delta Z_k + B_k \delta\tau_k \quad (12)$$

Based on the linearized model and tracking trajectories, the minimized cost function is given by[15]:

$$J(t) = \frac{1}{2} \{ [e^T(t)e(t)] + \int_{t-T}^t r\tau^T \tau d\sigma \} \quad (13)$$

where $r = 0.0001$. Therefore the control output τ is given as:

$$\tau_{k+1} = \tau_k + \delta\tau_k \quad (14)$$

where $\delta\tau_k$ is updated by the following set of equations:

$$\begin{aligned} \delta\tau_k &= -K\delta Z_k - K_v v_{k+1} - K_u \tau_k, \\ K &= (B_k^T S_{k+1} B_k + R)^{-1} B_k^T S_{k+1} A_k, \\ K_v &= (B_k^T S_{k+1} B_k + R)^{-1} B_k^T \\ K_u &= (B_k^T S_{k+1} B_k + R)^{-1} R \\ S_{k+1} &= A_k^T S_k (A_k - B_k K) + Q \\ v_{k+1} &= (A_k - B_k K)^T v_k - K^T R \tau_k + Q Z_k \end{aligned} \quad (15)$$

The parameters (e.g., R) and detailed description of the iLQR can be seen in [15], [14].

C. Operational Space Control (OSC)

Rewriting Eq.(1) while cancelling out the centripetal and Coriolis term in operational space [11]:

$$\tau = J_{ee}^T(q) M_{ee}(q) \ddot{x}_d + G(q) \quad (16)$$

with

$$\begin{aligned} M_{ee}(q) &= [J_{ee}(q) M^{-1}(q) J_{ee}^T(q)]^{-1}, \\ M(q) &= \sum_{i=0}^1 J_i^T(q) M_{x_i}(q) J_i(q), \\ M_{x_i} &= \begin{bmatrix} m_i & 0 & 0 & 0 \\ 0 & m_i & 0 & 0 \\ 0 & 0 & I_{xx} & I_{xy} \\ 0 & 0 & I_{yx} & I_{yy} \end{bmatrix}, \\ G(q) &= \sum_{i=0}^1 J_i^T(q) F_{g_i}, \end{aligned} \quad (17)$$

where $J_{ee}(q)$ is the Jacobian matrix of the end-effector of the human arm (see Eq.22). $m_{0,1}$ the masses of the joint center of mass (COM) (see Table I), $J_{0,1}(q)$ are the Jacobian matrices of the joint COM, $I_{xx,xy,yx,yy}$ the moments of inertia, and $F_{g_{0,1}}$ are the gravity forces on the arm segments (see Table I). Defining a basic PD controller in the Cartesian space:

$$\ddot{q}_d = k_p(q_d - q) + k_v(\dot{q}_d - \dot{q}), k_v = 9, k_v = \sqrt{k_p} \quad (18)$$

Substituting Eq.(18) into Eq.(16):

$$\tau = J_{ee}^T(q) M_{ee}(q) [k_p(q_d - q) + \sqrt{k_p}(\dot{q}_d - \dot{q})] + G(q) \quad (19)$$

The detailed description of the OSC can be seen in [11], [12].

III. EXPERIMENTS

The three controllers (described above) were implemented for achieving motor control tasks by using a physically simulated two-link arm. The arm is modelled after the human arm (see Fig. 2 and Table I) and built using MAPLESIM [11], [12]. The performance of the controllers are measured by the position error rate ζ and real ran time RT :

$$\zeta = \frac{\sum_{t=0}^T [\sqrt{(x(t) - x_d(t))^2 + (y(t) - y_d(t))^2}]}{N * dis}, N = \frac{T}{0.01} \quad (20)$$

where dis is the travelled distance of a desired trajectory (x_d, y_d) , T the time of task execution with time step $\Delta t = 0.01$, and N is the amount of its ran steps. The three controllers and their real ran time RT were ran and measured in a laptop (DELL Latitude E7470), respectively. The experiments of spatial-temporal adaptation refer to

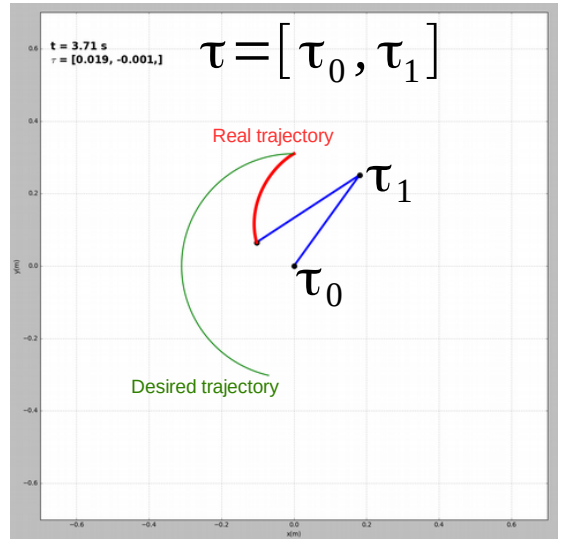


Fig. 2. A physically simulated human arm [11], [12]. Its geometry parameters are took from [16] (see Table I).

human motor control experiments [8], [7]. The tasks of multiple direction reaching and circular trajectory tracking were performed using the three controllers, respectively. For directional reaching, there were the 8 reaching targets in the 8 directions separated by 45° with the distance of $0.10(m)$. The required reaching time of each target is fixed, i.e., $T = 0.5(s)$. For circular trajectory tracking, the center of the circular trajectory is $[x = 0.00, y = 0.00](m)$ with the radius of $0.30(m)$ and the tracking time $T = 8(s)$. Note that the time T of task execution is the same for the three controller in a task, but their real ran time RT differs owing to their computation efficiency.

We can see that the proposed AMC and implemented iLQR succeeded in the human-like 8-target reaching (see the red and blue lines in Fig. 3 (A)), compared to the implemented OSC. This is because the AMC and iLQR allow for the larger joint torques (e.g., see the shoulder torque in Fig. 3 (B)) owing to online parameter adaptation. However, the AMC's parameter adaptation makes for more stable and smoother joint torques, compared to the iLQR. Such joint torques result from the force and impedance adaptation (see the red lines in Figs. 3 (C)-(E)) derived from Lyapunov stability (see Eq.8). Moreover, the iLQR failed to achieve the circular movement tracking (see the blue line in Fig. 3 (F)), while the AMC succeeded due to the larger and smoother joint torques (e.g., see the red line in Fig. 3 (G)). Such joint torques arise from online force and impedance adaptation based on the same adaptation law (see Eq.8) used in the directional reaching task. However,

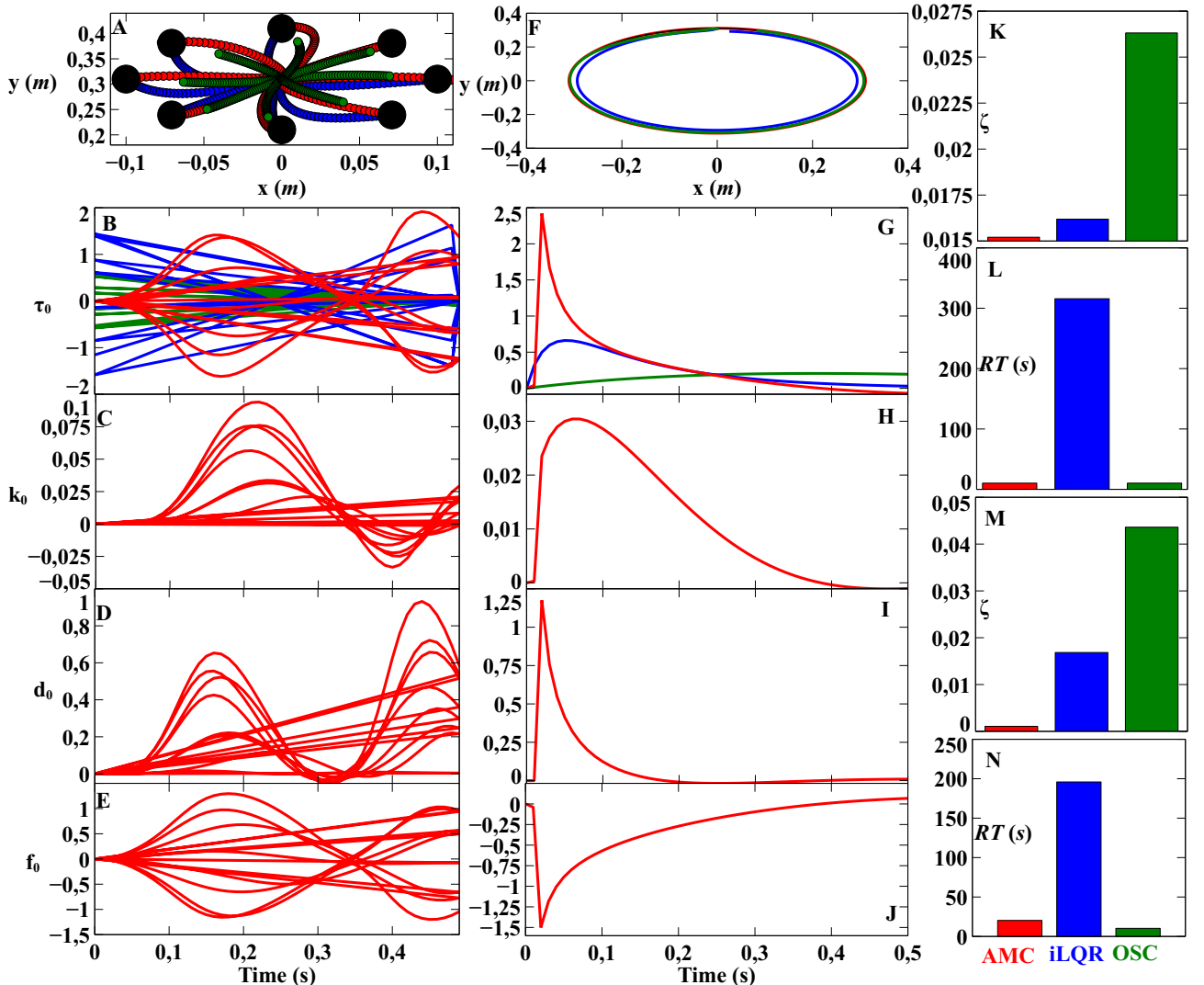


Fig. 3. Human-like motor behaviors resulted from the AMC, iLQR, and OSC. (A)-(E) and (K)-(L) depict the results of the 8-target reaching, while (F)-(J) and (M)-(N) show the results of the circular trajectory tracking. (A) The reaching trajectories (x, y) by the three controllers. (B) Shoulder joint torques τ_0 by the three controllers. (C) - (D) Stiffness $k_0(t)$, damping $d_0(t)$, force (f_0) adaptation by the AMC (see Eqs.(4) and (2)). The parameter adaptation follows Eq.(8). (F) The tracking trajectories (x, y) by the three controllers. (G) Shoulder joint torques τ_0 by the three controllers. (H) - (J) Stiffness $k_0(t)$, damping $d_0(t)$, force (f_0) adaptation by the AMC (see Eqs.(4) and (2)). The parameter adaptation follows Eq.(8). (K)-(N) The position error rates ζ and run time RT for the 8-target reaching and circular tracking (see Eq.(20), respectively. Black solid circles: reached targets; red lines and bars: AMC; blue lines and bars: iLQR; green lines and bars: OSC.

its adaptation amplitudes and patterns differ from those in the directional reaching task. For example, larger impedance and force were required in the initial period of the circular tracking task (see Figs. 3 (H)-(J)), while similar impedance and force occurred in the middle and end periods of the directional reaching (see Figs. 3(C)-(E)). Such adaptations result in more accurate reaching and tracking behaviors (i.e., less position error rate ζ , see Figs. 3 (K) and (M)), compared to the implemented iLQR and OSC. Furthermore, one can see that computation of the iLQR are much more expensive (see Figs. 3 (L) and (N)) than those of the AMC and OSC due to its complex control law (see Eq.15). The video clip can be seen at <https://www.youtube.com/watch?v=gldRGmZJyI8>. The AMC still succeeded in more irregular (i.e., star) trajectory tracking tasks that the implemented OSC

and iLQR failed in. This is because its law (see Eq.8) makes for the amplitude and frequency of the force and impedance parameters (see Eqs.(4) and (2)) in a variety of motor control tasks (see the adaptation comparison in Figs. 4 (C)-(E)). The video clip can be seen at <https://www.youtube.com/watch?v=xzwwRoXZozs>. Taken together the AMC can produce more accurate and stable human-like motor behaviors (e.g., real time trajectory tracking), compared to the implemented iLQR and OSC.

IV. CONCLUSIONS

The proposed AMC is a biomimetic controller allowing for online force and impedance in various motor control tasks. Its simple adaptation law could be applied to online adaptive control in bio-mechatronic devices (e.g., prostheses). On the

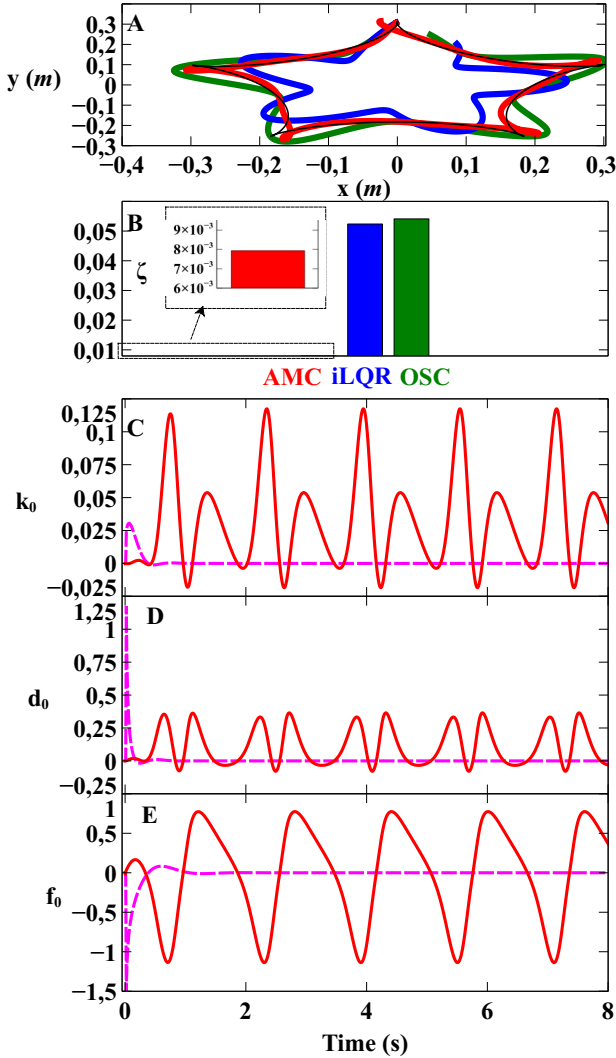


Fig. 4. Irregular trajectory tracking. (A) The tracking trajectories (x, y) by the three controllers. (B) The position error rates ζ . (C)-(E) The comparison of the stiffness $k_0(t)$, damping $d_0(t)$, force (f_0) adaptation in the circular and irregular tracking. The parameter adaptation follows Eq.8. Red solid lines: Irregular tracking; magenta dashed line: circular tracking (the same as those in Figs.3 (H) - (J)).

another hand, it can be extended to solve a problem of inverse dynamics adaptation in high DOF robots.

APPENDIX

A. Kinematic and Geometry of the Human Arm

The position (x, y) the arm end-effector is be given by:

$$\begin{bmatrix} x \\ y \end{bmatrix} = \begin{bmatrix} L_0 \cos(q_0) + L_1 \cos(q_0 + q_1) \\ L_0 \sin(q_0) + L_1 \sin(q_0 + q_1) \end{bmatrix} \quad (21)$$

and its Jacobian matrix is given by:

$$J_{ee}(q) = \begin{bmatrix} -L_0 \sin(q_0) - L_1 \sin(q_0 + q_1) & -L_1 \sin(q_0 + q_1) \\ L_0 \cos(q_0) + L_1 \cos(q_0 + q_1) & L_1 \cos(q_0 + q_1) \end{bmatrix} \quad (22)$$

TABLE I

PARAMETERS OF THE TWO LINK ARM OF FIG. 1 [16]

Arms	Upper	Fore
Masses (kg)	1.93	1.52
Lengths (m)	0.31	0.34
Centers of mass from proximal joint (m)	0.165	0.19
Mass moments of inertia (kgm^2)	0.0141	0.0188

B. Adaptation Law of AMC

Let $F_E(t)$, $K_E(t)$, and $D_E(t)$ (see Eq.(8)) be the expected force, stiffness, and damping matrices for achieving stable joint motions and task adaptation:

$$\tilde{F} = F - F_E, \tilde{K} = K - K_E, \tilde{D} = D - D_E \quad (23)$$

Combining with Eq.5 yields

$$J_c(t) = \frac{1}{2} \int_{t-T}^t \text{vec}^T(\tilde{K}) Q_k^{-1} \text{vec}(\tilde{K}) + \text{vec}^T(\tilde{D}) Q_d^{-1} \text{vec}(\tilde{D}) + \tilde{F}^T Q_f^{-1} \tilde{F} d\sigma \quad (24)$$

where Q_f , Q_k , and Q_d are symmetric positive-definite matrices, and $\text{vec}(\cdot)$ stands for the column vectorization. Now, Eqs.8 can be written as:

$$\begin{aligned} \delta \tilde{F}(t) &= Q_f[\varepsilon(t) - \gamma(t)F(t)] \rightarrow 0, t \rightarrow \infty \\ \delta \tilde{K}(t) &= Q_k[\varepsilon(t)e^T(t) - \gamma(t)K(t)] \rightarrow 0, t \rightarrow \infty \\ \delta \tilde{D}(t) &= Q_d[\varepsilon(t)\dot{e}^T(t) - \gamma(t)D(t)] \rightarrow 0, t \rightarrow \infty \end{aligned} \quad (25)$$

where all functions are unknown and periodic with T . Consider the difference between $J_c(t)$ (see Eq.24) of two consecutive periods:

$$\begin{aligned} \delta J_c &= J_c(t) - J_c(t-T) \\ &= \frac{1}{2} \int_{t-T}^t \text{tr}\{\tilde{K}^T(\sigma) Q_k^{-1} \tilde{K}(\sigma) - \tilde{K}^T(\sigma-T) Q_k^{-1} \tilde{K}(\sigma-T)\} \\ &\quad + \text{tr}\{\tilde{D}^T(\sigma) Q_d^{-1} \tilde{D}(\sigma) - \tilde{D}^T(\sigma-T) Q_d^{-1} \tilde{D}(\sigma-T)\} \\ &\quad + \text{tr}\{\tilde{F}^T(\sigma) Q_f^{-1} \tilde{F}(\sigma) - \tilde{F}^T(\sigma-T) Q_f^{-1} \tilde{F}(\sigma-T)\} d\sigma \end{aligned} \quad (26)$$

where $\text{tr}\{\cdot\}$ stands for the trace of a matrix. Using the symmetry of Q_k^{-1} and Eq.(25), the first term of Eq.(26) can be written as:

$$\begin{aligned} &\text{tr}\{\tilde{K}^T(\sigma) Q_k^{-1} \tilde{K}(\sigma) - \tilde{K}^T(\sigma-T) Q_k^{-1} \tilde{K}(\sigma-T)\} \\ &= \text{tr}\{[\tilde{K}^T(\sigma) - \tilde{K}^T(\sigma-T)] Q_k^{-1} \\ &\quad \times [2\tilde{K}^T(\sigma) - \tilde{K}^T(\sigma) + \tilde{K}^T(\sigma-T)]\} \\ &= \text{tr}\{\delta \tilde{K}^T(\sigma) Q_k^{-1} [2\tilde{K}^T(\sigma) - \delta \tilde{K}(\sigma)]\} \\ &= -\text{tr}\{\delta \tilde{K}^T(\sigma) Q_k^{-1} \delta \tilde{K}(\sigma)\} + 2\text{tr}\{\delta \tilde{K}^T(\sigma) Q_k^{-1} \tilde{K}^T(\sigma)\} \\ &= -\text{tr}\{\delta \tilde{K}^T(\sigma) Q_k^{-1} \delta \tilde{K}(\sigma)\} \\ &\quad + 2\varepsilon(\sigma) \tilde{K}(\sigma) e(\sigma) - 2\gamma(\sigma) \text{tr}\{\tilde{K}^T(\sigma) \tilde{K}(\sigma)\} \end{aligned} \quad (27)$$

Then, similarly, the second and third terms can be:

$$\begin{aligned} &\text{tr}\{\tilde{D}^T(\sigma) Q_d^{-1} \tilde{D}(\sigma) - \tilde{D}^T(\sigma-T) Q_d^{-1} \tilde{D}(\sigma-T)\} \\ &= -\text{tr}\{\delta \tilde{D}^T(\sigma) Q_d^{-1} \delta \tilde{D}(\sigma)\} \\ &\quad + 2\varepsilon(\sigma) \tilde{D}(\sigma) \dot{e}(\sigma) - 2\gamma(\sigma) \text{tr}\{\tilde{D}^T(\sigma) \tilde{D}(\sigma)\} \end{aligned} \quad (28)$$

$$\begin{aligned} & \text{tr}\{\tilde{F}^T(\sigma)Q_f^{-1}\tilde{F}(\sigma) - \tilde{F}^T(\sigma-T)Q_f^{-1}\tilde{F}(\sigma-T)\} \\ &= -\text{tr}\{\delta\tilde{F}^T(\sigma)Q_f^{-1}\delta\tilde{F}(\sigma) \\ &+ 2\varepsilon(\sigma)\tilde{F}(\sigma) - 2\gamma(\sigma)\text{tr}\{\tilde{F}^T(\sigma)\tilde{F}(\sigma)\} \end{aligned} \quad (29)$$

Substituting Eqs.(27), (28), and (29) into Eq.(26):

$$\begin{aligned} \delta J_c = & -\frac{1}{2} \int_{t-T}^t \delta\tilde{\Phi}^T(\sigma)Q^{-1}\delta\tilde{\Phi}(\sigma)d\sigma \\ & - \int_{t-T}^t \gamma(\sigma)\tilde{\Phi}^T(\sigma)\tilde{\Phi}(\sigma)d\sigma \\ & + \int_{t-T}^t \varepsilon(\sigma)\tilde{K}(\sigma)e(\sigma) + \varepsilon(\sigma)\tilde{D}(\sigma)\dot{e}(\sigma) + \varepsilon(\sigma)\tilde{F}(\sigma)d\sigma \end{aligned} \quad (30)$$

where the matrices $\tilde{\Phi}(t)$ and Q are given by:

$$\begin{aligned} \tilde{\Phi}(t) &= [\text{vec}(\tilde{K}(t))^T, \text{vec}(\tilde{D}(t))^T, \tilde{F}(t)]^T \\ Q &= \text{diag}(I \otimes Q_k, I \otimes Q_d, Q_f) \end{aligned} \quad (31)$$

Similarly, using the skew symmetry of the matrix $\dot{M} - 2C$, Eqs.(1) and (23), δJ_p of Eq.(6) can be written by:

$$\begin{aligned} \delta J_p &= J_p(t) - J_p(t-T) \\ &= - \int_{t-T}^t \varepsilon(\sigma)\tilde{K}(\sigma)e(\sigma) + \varepsilon(\sigma)\tilde{D}(\sigma)\dot{e}(\sigma) + \varepsilon(\sigma)\tilde{F}(\sigma)d\sigma \end{aligned} \quad (32)$$

Combining Eqs.(30) and (32), the derivative δJ of Eq.(7) can be given by:

$$\begin{aligned} \delta J &= J(t) - J(t-T) = \delta J_c + \delta J_p \\ &= -\frac{1}{2} \int_{t-T}^t \delta\tilde{\Phi}^T(\sigma)Q^{-1}\delta\tilde{\Phi}(\sigma)d\sigma \\ & - \int_{t-T}^t \gamma(\sigma)\tilde{\Phi}^T(\sigma)\tilde{\Phi}(\sigma)d\sigma \end{aligned} \quad (33)$$

A sufficient condition for $\delta J \leq 0$ is that Q^{-1} is a positive-definite matrix and,

$$\gamma(\sigma) > 0, \tilde{\Phi}^T\tilde{\Phi} \geq 0. \quad (34)$$

The scalars a and b in $\gamma(t)$ are set as:

$$a = 0.2, b = 5 \quad (35)$$

ACKNOWLEDGMENT

The authors would like to thank Travis DeWolf, Dario Farina, Massimo Sartori, Jianwei Zhang, Görner Michael, Kerzel Matthias, and John Hallam for their help and consultation.

REFERENCES

- [1] David W Franklin, Etienne Burdet, Keng Peng Tee, Rieko Osu, Chee-Meng Chew, Theodore E Milner, and Mitsuo Kawato. CNS Learns Stable, Accurate, and Efficient Movements Using a Simple Algorithm. *The Journal of Neuroscience*, 28(44):11165 LP – 11173, oct 2008.
- [2] Etienne Burdet, Gowrishankar Ganesh, Chenguang Yang, and Alin Albu-Schäffer. Interaction Force, Impedance and Trajectory Adaptation: By Humans, for Robots. In Oussama Khatib, Vijay Kumar, and Gaurav Sukhatme, editors, *Springer Tracts in Advanced Robotics*, pages 331–345. Springer Berlin Heidelberg, Berlin, Heidelberg, - experime edition, 2014.
- [3] C Yang, G Ganesh, S Haddadin, S Parusel, A Albu-Schaeffer, and E Burdet. Human-Like Adaptation of Force and Impedance in Stable and Unstable Interactions. *IEEE Transactions on Robotics*, 27(5):918–930, 2011.
- [4] Alex M C Smith, Chenguang Yang, Hongbin Ma, Phil Culverhouse, Angelo Cangelosi, and Etienne Burdet. Novel Hybrid Adaptive Controller for Manipulation in Complex Perturbation Environments. *PLOS ONE*, 10(6):e0129281, jun 2015.
- [5] Jonas Buchli, Freek Stulp, Evangelos Theodorou, and Stefan Schaal. Learning variable impedance control. *The International Journal of Robotics Research*, 30(7):820–833, apr 2011.
- [6] K Kronander and A Billard. Stability Considerations for Variable Impedance Control. *IEEE Transactions on Robotics*, 32(5):1298–1305, 2016.
- [7] Abdelhamid Kadiallah, David W Franklin, and Etienne Burdet. Generalization in Adaptation to Stable and Unstable Dynamics. *PLOS ONE*, 7(10):e45075, oct 2012.
- [8] Michael A Conditt, Francesca Gandolfo, and Ferdinando A Mussa-Ivaldi. The Motor System Does Not Learn the Dynamics of the Arm by Rote Memorization of Past Experience. *Journal of Neurophysiology*, 78(1):554–560, jul 1997.
- [9] Aravind Rajeswaran, Kendall Lowrey, Emanuel V Todorov, and Sham M Kakade. Towards Generalization and Simplicity in Continuous Control. In I Guyon, U V Luxburg, S Bengio, H Wallach, R Fergus, S Vishwanathan, and R Garnett, editors, *Advances in Neural Information Processing Systems 30*, chapter Rajeswaran, pages 6550–6561. Curran Associates, Inc., 2017.
- [10] Michael Mistry and Ludovic Righetti. Operational Space Control of Constrained and Underactuated Systems. In *Proceedings of Robotics: Science and Systems*, Los Angeles, CA, USA, 2011.
- [11] Travis DeWolf. *A neural model of the motor control system*. Phd thesis, University of Waterloo, 2014.
- [12] Travis DeWolf, Terrence C Stewart, Jean-Jacques Slotine, and Chris Eliasmith. A spiking neural model of adaptive arm control. *Proceedings of the Royal Society B: Biological Sciences*, 283(1843), nov 2016.
- [13] David Braun, Matthew Howard, and Sethu Vijayakumar. Optimal variable stiffness control: formulation and application to explosive movement tasks. *Autonomous Robots*, 33(3):237–253, 2012.
- [14] Y Tassa, N Mansard, and E Todorov. Control-limited differential dynamic programming. In *2014 IEEE International Conference on Robotics and Automation (ICRA)*, pages 1168–1175, 2014.
- [15] Weiwei Li and Emanuel Todorov. Iterative Linear Quadratic Regulator Design for Nonlinear Biological Movement Systems. In *International Conference on Informatics in Control, Automation and Robotics*, 2004.
- [16] E Burdet, K P Tee, I Mareels, T E Milner, C M Chew, D W Franklin, R Osu, and M Kawato. Stability and motor adaptation in human arm movements. *Biological Cybernetics*, 94(1):20–32, 2006.
- [17] J McIntyre, F A Mussa-Ivaldi, and E Bizzi. The control of stable postures in the multijoint arm. *Experimental Brain Research*, 110(2):248–264, 1996.
- [18] Keng Peng Tee, David W Franklin, Mitsuo Kawato, Theodore E Milner, and Etienne Burdet. Concurrent adaptation of force and impedance in the redundant muscle system. *Biological Cybernetics*, 102(1):31–44, 2010.
- [19] N Hogan. On the stability of manipulators performing contact tasks. *IEEE Journal on Robotics and Automation*, 4(6):677–686, 1988.